ADVANCED ENGINEERING MATERIALS
www.aem-journal.com

# Digital Machine Knitted Resistive Strain Sensor for Wireless Human Motion Monitoring

*Safi Ahmed, Md. Mohaddesh Hosen,* Abdullah Al Saif, and Md. Tanvir Ahmed Khandaker*

**Textile-based wearable sensors are gaining popularity in healthcare and soft robotics due to their rapid, scalable, and low-cost production. Among them, strain sensors have been drawing attention in various human motion detection and health monitoring applications. In this article, knitted strain sensors based on interlock structures have been fabricated for capturing human movement and their remote monitoring. To achieve high stretchability and electrical stability, elastic core spun (nylon/PU) with conductive (polyester/stainless steel) yarn has been realized to prototype the sensors. Six different samples with different yarn variations have been extensively investigated by various electromechanical characterizations. The developed strain sensors show a maximum gauge factor of 3.04 with excellent linearity ($R^2 = 0.9911$) and remarkable durability of 1500 cycles. These sensors also demonstrate rapid response (≈80 ms) and recovery time (≈120 ms) and exhibit good performance after 10 wash cycles, assessing the real-world application of the sensors. To validate the applicability of the strain sensors in human motion monitoring, an elbow support guard and a kneecap have been constructed to demonstrate bending angle detection as well as wireless monitoring of various human locomotion. The developed strain sensors hold immense possibilities in health monitoring, physical rehabilitation, and sports applications.**

## 1. Introduction

In recent years, conventional textiles combined with wearable sensors have made revolutionary steps due to their comfort, flexibility, conformability, versatility, breathability, and skin adhesion characteristics.[1–3] Integrating ordinary hardware into textiles can be challenging due to its inflexibility and weight.[4,5] This is why sensing materials are incorporated into textiles in a seamless manner,[6,7] which allows for the distribution of these materials evenly over the cloth and boosts the durability and washability properties of e-textiles.[8–10] Wearable e-textiles can capture electrical changes occurring from activities of synovial joints[11] as well as physiological activities[12,13] such as heartbeat,[13] pulse,[14] muscular activity,[15] respiration,[14,16] sweat,[17] and body temperature,[13,18] which are vastly used in soft robotics,[19] biomedical,[12] physiotherapy,[20] sports,[21] and military applications.[22] It is possible to fabricate wearable sensors by incorporating the conductive materials into the textile through knitting,[23–25] weaving,[26] braiding,[22] embroidery,[27] sewing,[21] screen printing,[28] inkjet printing,[29] or coating.[11] However, the challenge lies in manufacturing these sensors in a scalable and cost-effective manner[30] while also ensuring their performance[31] in terms of sensitivity, durability, washability, and repeatability. Knit-based sensor fabrication, especially flatbed knitting, is gaining popularity because of its ability to provide rapid prototyping as well as mass manufacturing of flexible sensors.[2]

When monitoring limb activities, the movement of joints undergoes a significant change, necessitating the use of sensors capable of substantial stretching and recovery to their original position. This extension and recovery phenomenon can be detected more extensively and effortlessly in strain sensors than in pressure sensors.[32–34] Textile-based strain sensors can be classified based on their capability of converting physical and mechanical changes in the human body into electrical signals, that is, resistance,[15,35] capacitance,[36] inductance,[37,38] piezoelectric,[39] and triboelectric signals.[40,41] Compared to other sensing principles, resistive strain sensors provide higher sensitivity, which is important for applications where large deformation occurs, that is, elbow and knee bending for human motion monitoring.[42,43] The fabric structure and the sensing materials to be employed play a crucial role in terms of performance when it comes to fabricating knitted strain sensors. In flatbed knitting, various knitting structures such as single jersey,[23,44] rib structures,[45,46] and spacer fabrics,[6,47,48] have been explored in previous studies. However, to the best of our knowledge, there has been limited exploration of strain sensors based on interlock structures.

Knitted resistive strain sensors generally comprise two types of yarns, that is, conductive functional yarn and nonconductive base yarn. A wide range of materials, including cotton, polyester, nylon, acrylic, polyurethane, etc., are used as base materials. Elastomeric yarns such as core-sheath configuration and spandex have been incorporated along with the nonconductive base

S. Ahmed, M. M. Hosen, A. A. Saif, M. T. A. Khandaker
Department of Fabric Engineering
Bangladesh University of Textiles
92, Shahid Tajuddin Ahmed Sarani, Dhaka 1208, Bangladesh
E-mail: mohaddesh@fe.butex.edu.bd

The ORCID identification number(s) for the author(s) of this article can be found under https://doi.org/10.1002/adem.202502090.

**DOI: 10.1002/adem.202502090**

 

materials to enhance the durability and stability of the strain sensors.[23] Typically, highly sensitive functional yarns, including carbon nanotube (CNT)-wrapped yarns,[49,50] graphene,[48,51] and conductive polymer yarns like polypyrrole[36] and PEDOT:PSS,[52] have been extensively used in fabricating wearable strain sensors. However, these materials often tend to be costly, and their fabrication process is not easily scalable.[53–55] Some literature has demonstrated the fabrication of strain sensors in a scalable way using metal particle-based yarns such as silver[45,56] and stainless steel[57] based conductive yarns. Rumon et al. developed a knitted strain sensor based on silver-coated polyamide yarn for monitoring respiration, which exhibited a relatively lower sensitivity and linearity.[16] In another work, a stitched-based strain sensor was developed using silver-plated conductive thread for sports and fitness analysis, but it lacked durability and sensitivity.[21] Seyedin et al. used PU/PEDOT:PSS conductive polymers as functional components to develop knitted strain sensors for detection of knee bending at 0° and 90°.[58] These sensors, which were developed using low-cost functional materials, exhibit various limitations, such as lower sensitivity, linearity, durability, and limited applications. Yilmaz et al. developed a machine knitted capacitive strain sensor-based knee brace for human motion monitoring[59] where they used an additional MPR121 for capacitive data collection along with an Arduino-based microcontroller, which may hinder wearability.

In this work, resistive strain sensors based on interlock weft-knit structure have been realized using PES/stainless steel conductive yarn and nonconductive nylon-wrapped polyurethane yarn. A computerized flatbed knitting machine was utilized for the seamless integration of sensing materials into the base fabric for wearable sensing applications. The use of wrapped elastic yarn proved to be vital in improving the mechanical stability of the sensors. During the characterization of the developed sensors, they exhibited satisfactory sensitivity in terms of both the gauge factor and linearity. The durability of the sensors was inspected by conducting cyclic strain tests consisting of 1500 cycles of constant stretching and releasing. It was also concluded that the conductivity of the sensors was stable after numerous washing cycles, deeming them appropriate for further commercial wearable applications. Finally, as a proof of concept, the developed sensor was integrated into an elbow guard and kneecap to demonstrate the applicability of the sensor via wireless data transmission and real-time visualization for various human locomotion, that is, walking, jogging, running, cycling, etc.

## 2. Results and Discussion

### 2.1. Overview of the Knitted Strain Sensor

**Figure 1**a shows the development workflow of the resistive strain sensor. The knitted strain sensor was developed using a computerized flat knitting machine (Shima Seiki SSR112_14G, 45-inch knitting width, single R2 carriage knitting system, Sakata Wakayama, Japan), which provides seamless integration of conductive yarns into the base fabric. At first, a 2 × 2 interlock knit structure was designed using the KnitPaint Module of the Shima Seiki SDS One APEX 3 software. The knitting program designed for the sensor is depicted in Figure 1b. The main structure of the fabric is elucidated in the middle portion, whereas the vertical lines on either side, referred to as option lines, represent various machine commands. The Apex 3 software generates a machine code to provide precise instructions to the knitting machine concerning the fabrication of the sensor. The Shima Seiki SSR112 flat knitting machine consists of 9 carriers. Three carriers were used to fabricate the sensor: one for the conductive yarn, one for the base yarn, and one for waste knitting. After several iterations on various interlock-based structures, the 2 × 2 interlock structure (Figure 1c) was chosen because this knitting structure provides better recovery after stretching compared to other knitting structures.

Figure 1d represents a view of the fabricated sensor in the machine during simultaneous movement of the front and back bed needles. During the fabrication of the sensors, the conductive PES/stainless steel yarns were integrated into the 2 × 2 interlock structure in a course-wise pattern along with the base material. The conductive yarns can be integrated into the sensor by various means. After multiple iterations, six combinations were chosen to characterize the knitted strain sensor, as shown in Figure S1, Supporting Information. The details of six knitted sensors are given in **Table 1**. The base material for all the sensors was constructed using nylon yarn doubled with nylon-wrapped spandex yarn. However, the main variations were in the sequences of conductive yarn stripes produced in the course direction using the conductive and nonconductive yarns. The stitch length of all the developed samples was ≈2.5 mm, with a stitch density of 38 courses per inch and 27 wales per inch. The carriage speed for knitting the sensor was set to 0.70 m s$^{-1}$. To prevent fabric pileup between the front and rear beds and ensure faultless fabrication, the takedown speed was also optimized using the appropriate monitor command.

### 2.2. Strain-Resistance Relationship

**Figure 2** shows the relationship between resistance and strain in the knitted strain sensor. To investigate the effect of strain on resistance, the sensor was stretched by 40% at 100 mm min$^{-1}$ crosshead speed. Previous works have used a strain range between ≈35% and ≈50% to characterize the resistance-strain profile.[59,60] However, our study shows that 40% strain is enough to capture normal daily activity movements for humans. For all sensor types, the resistance on the sensor decreases when the strain on the sensor increases. Figure 2a shows the strain-resistance relationship of sensor type 4. The strain-resistance profile of other sensor types is depicted in Figure S2, Supporting Information. This resistance dropping characteristics due to strain can be described by Holm's contact theory.[61]

$$R_C = \frac{\rho}{2}\sqrt{\frac{\pi H}{nP}} \tag{1}$$

here, $R_C$ = resistance of the sensor, $\rho$ = resistivity of the conductive yarn, $H$ = hardness of conductive yarn at contact point, $n$ = number of contact points, and $P$ = contact pressure.

For a textile-based structure, resistivity of materials ($\rho$) and material hardness ($H$) are constant, as shown in Equation (1). However, applying strain to a material increases the number

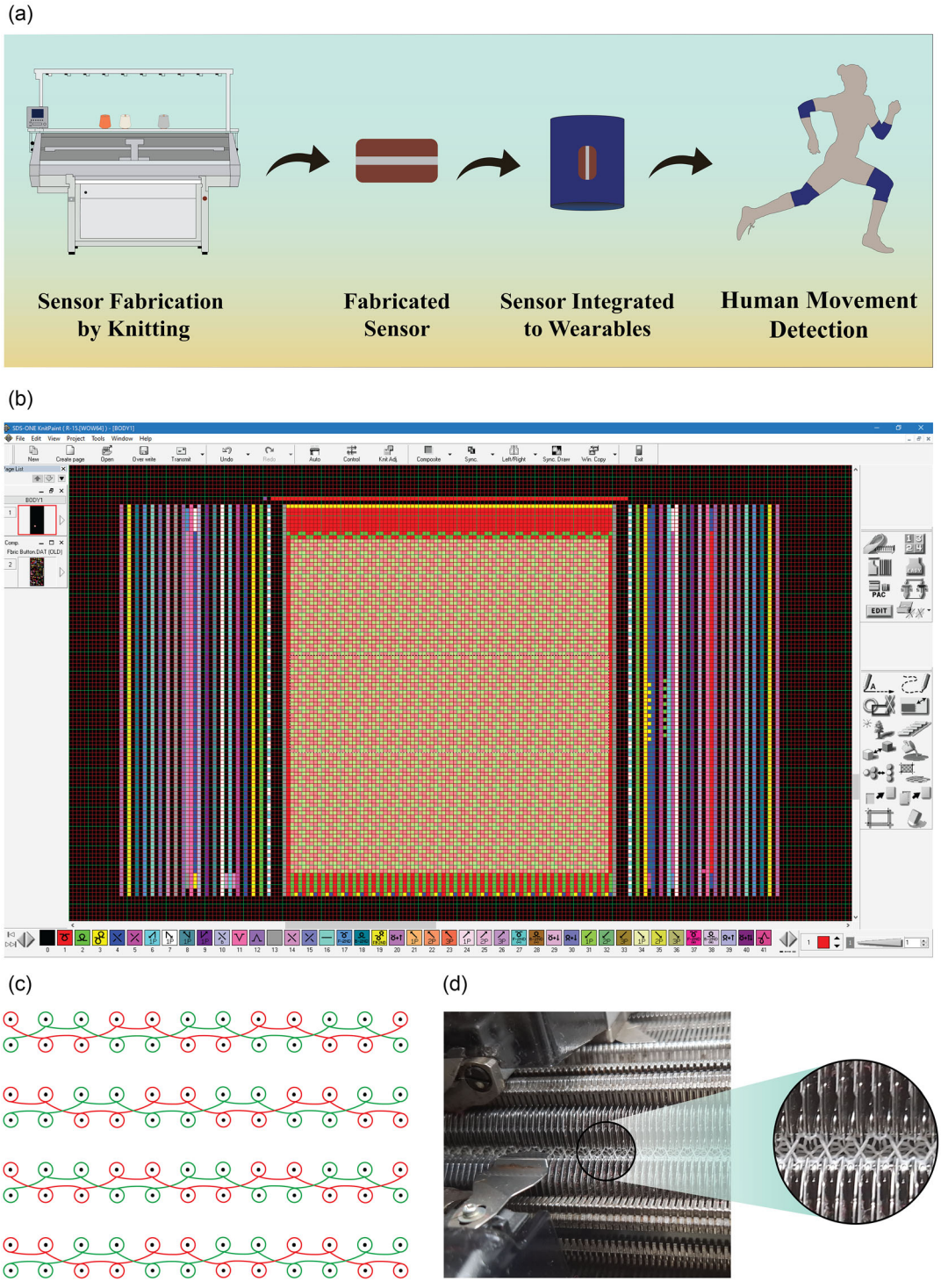


**Figure 1.** Fabrication of the resistive strain sensor. a) Operational sequence of the knitted strain sensor. b) Sensor design on the KnitPaint module of the Apex 3 software. c) Notation diagram of the 2 × 2 interlock knit structure. d) Needle bed view of the sensor during knitting.

of contact points ($n$) and the contact pressure ($P$), thereby decreasing resistance. When the applied strain is released, contact points ($n$) between the conductive path decrease again along with the contact pressure. This causes an increase in the resistance of the knitted sensor. The strain-resistance hysteresis curve (Figure 2b) shows the consecutive loading and unloading and their corresponding resistance change for sensor type 4. The strain-resistance hysteresis graph for all other sensor types is depicted in Figure S3, Supporting Information. Figure 2c shows the optical image of the sensor type 4 at 20× magnification

**Table 1.** Fabrication details of the developed samples.

| Sensor type | Conductive functional yarn | Sensor structure | |
|---|---|---|---|
| | | Conductive courses | Non-conductive courses |
| 1 | PES/SS yarn | 1 | 1 |
| 2 | PES/SS yarn | 2 | 1 |
| 3 | PES/SS yarn | 1 | 2 |
| 4 | PES/SS yarn + nylon-wrapped spandex yarn | 1 | 1 |
| 5 | PES/SS yarn + nylon-wrapped spandex yarn | 2 | 1 |
| 6 | PES/SS yarn + nylon-wrapped spandex yarn | 1 | 2 |

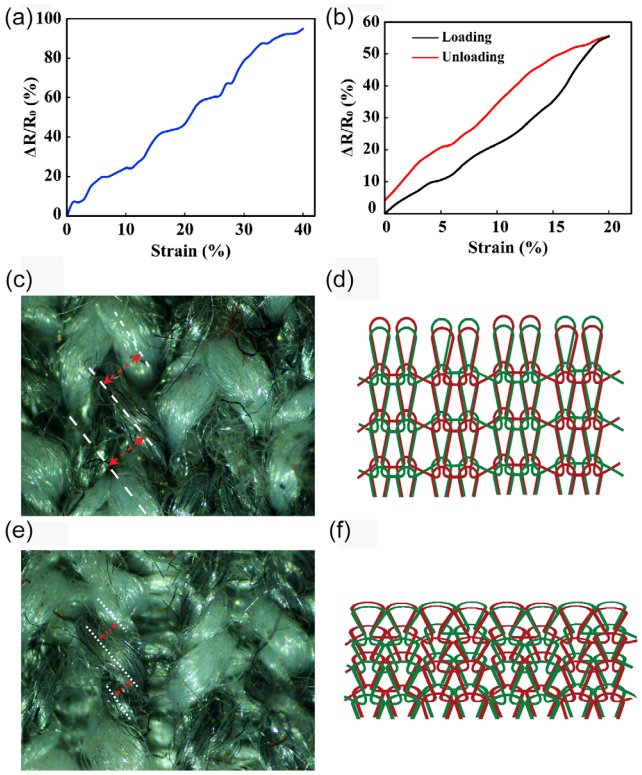


**Figure 2.** Effect of strain on the resistance of a knitted sensor. a) Strain-resistance relationship of sensor type 4. b) Hysteresis graph of sensor type 4. c) Microscopic view of the sensor during relaxed state, indicating significant loop-to-loop distance. d) Looping diagram of the sensor during relaxed state. e) Microscopic view of the sensor during stretched state (60% strain), demonstrating minimal loop-to-loop distance. f) Looping diagram of the sensor during stretched state.

during its relaxed state, and Figure 2d shows its corresponding looping diagram. When the sensor is not stretched, there is a gap between the adjacent loops. But when the sensor undergoes 60% strain, the loop-to-loop distance of the conductive yarn decreases as shown in Figure 2e and contributes to the resistance drop. The corresponding looping diagram of the knitted sensor when it is stretched in the course direction is shown in Figure 2f. The optical view under 20× magnification of sensor type 4 in 40% and 100% strain is given in Figure S4, Supporting Information. The similar phenomenon is also observed in those scenarios where the loop-to-loop distance gradually decreases when strain on the sensor increases.

### 2.3. Sensing Performance

The sensitivity of a knitted strain sensor is a critical factor in terms of its sensing performance, which is quantified by the gauge factor. The gauge factor is essentially the ratio of the change in resistance ($\Delta R$) to its initial resistance ($R_0$) divided by the strain ($\varepsilon$), as shown in Equation (2).

$$\text{Gauge factor} = \frac{\Delta R/R_0}{\varepsilon} \tag{2}$$

**Figure 3**a shows the gauge factors of all developed sensors. Here, sensor type 4 exhibits the maximum gauge factor compared to other sensor types. This improvement is attributed to the inclusion of the stretchable nylon-wrapped spandex yarn with the conductive yarn courses in sensor types 4, 5, and 6, which is not present in sensor types 1, 2, and 3, as shown in Table 1. Sensor types 1 and 4 contain the 1-course conductive yarn and 1-course nonconductive yarn combination, whereas sensor types 2 and 5 and sensor types 3 and 6 contain 2-course conductive, 1-course nonconductive, and 1-course conductive and 2-course nonconductive yarn combinations, respectively. These fabrication differences are reflected in the gauge factors of these sensor types. The 1 conductive and 1 nonconductive combination of sensor types 1 and 4 shows higher gauge factors than other combinations. However, sensor type 4 has a higher gauge factor of 3.04 compared to sensor type 1 (GF ≈ 2.72), which is on par with the existing knit-based strain sensors.[19,26,27]

An important factor for the applicability of a sensor in real-world applications is its linearity. As shown in Figure 3b, sensor types 4, 5, and 6 show higher linearity compared to the other ones. Again, this is due to the use of extra stretchable yarns with the conductive courses, which provided better mechanical stability (Figure S5, Supporting Information). Overall, sensor type 4 provided the highest linearity ($R^2 = 0.9911$).

The stability of the strain sensors under certain strain is one of the crucial properties of smart garments. Here each of the six distinct strain sensors was tested at a speed of 50 mm min$^{-1}$. The stepwise strain variation graphs explain the changes in resistance over time at various strain percentages, such as 0% (relaxed state), 10%, 20%, 30%, and 40%. The sensors were

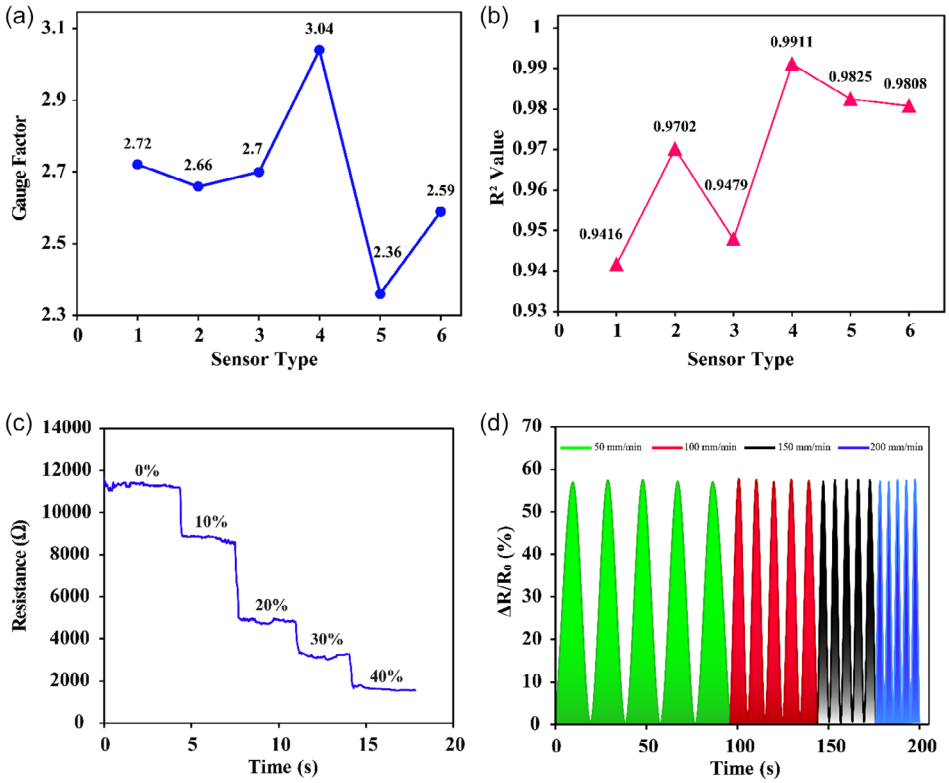


**Figure 3.** Sensing performance of the knitted strain sensors. a) Gauge factor of sensor types 1–6. b) Linearity of the knitted strain sensors. c) Stepwise resistance change of sensor type 4 at 10%, 20%, 30%, and 40% strain. d) Sensing performance of sensor type 4 under various strain speeds.

stretched incrementally by 10% and then held in place for ≈3–5 s until 40% strain was obtained. Figure 3c depicts the stepwise increase of strain result for sensor type 4, which exhibits that the change in resistance is almost similar in all strain intervals between 0% and 40%. As a result, the knitted strain sensor is able to sense stretching stimuli precisely under different conditions and convert them into electrical signals, which is elaborated in the application section. Other sensor types exhibit almost similar phenomena, as shown in Figure S6, Supporting Information.

Another test that represents the stability of knitted strain sensors is the variable-speed cyclic test. One of the key challenges of strain sensors is maintaining a consistent electrical response, that is, resistance, under repeated deformation. Here, the changes in relative resistance at 20% strain were measured at crosshead speeds of 50, 100, 150, and 200 mm $min^{-1}$. Sensor type 1 (Figure S7a, Supporting Information) and sensor type 4 (Figure 3d) exhibit consistent resistance and overall stability compared to other developed sensors, as shown in Figure S7b–e, Supporting Information.

The response-recovery test is performed to evaluate the time it takes to visualize the change in electrical signal during the deformation of the knitted strain sensor. The response time denotes the time it takes to change the electrical signal when mechanical strain occurs, whereas the recovery time indicates similar variation in time but during its recovery to the original state. To perform the response-recovery test, sensor type 4 was stretched at 5% strain at 500 mm $min^{-1}$ crosshead speed and was released back to its initial state after a few seconds. **Figure 4**a shows the response and recovery time of sensor type 4, which are 80 ms and 120 ms, respectively. A lower response and recovery time demonstrate the suitability of the sensor for human locomotion monitoring applications.

In addition to establishing electromechanical stability, the washability test helps to identify whether there are any broken or damaged loops, excessive abrasion, pilling, or other issues after several wash cycles. These issues are often responsible for the decline in the sensing performance of knitted strain sensors. The test was carried out according to the BS EN standard test protocol ISO 105-C10. A laundry machine was used to introduce mechanical agitation, accompanied by water and commercial washing detergent for washing. In a total of 10 washing cycles, the dynamic changes in resistance at relaxed state, 20%, and 40% strain were measured after each pair of wash cycles. Figure 4b depicts the resistance variance after 10 washes for sensors of type 4. It can be observed that the resistance values remain stable up to eight wash cycles but increase significantly after 10 washes. In fact, the resistance value during 40% strain reduces slightly after six washes, followed by a gradual increase after that. One possible reason for this variability could be the disturbance in the contact point of the loops due to mechanical agitation.[62,63] As for sensor types 1 and 2 (Figure S8a,b, Supporting Information), resistance values after washing behaved similarly by showing stable resistance up to eight wash cycles and then increasing drastically after 10 wash cycles. Compared to sensor types 1, 2, and 4, the

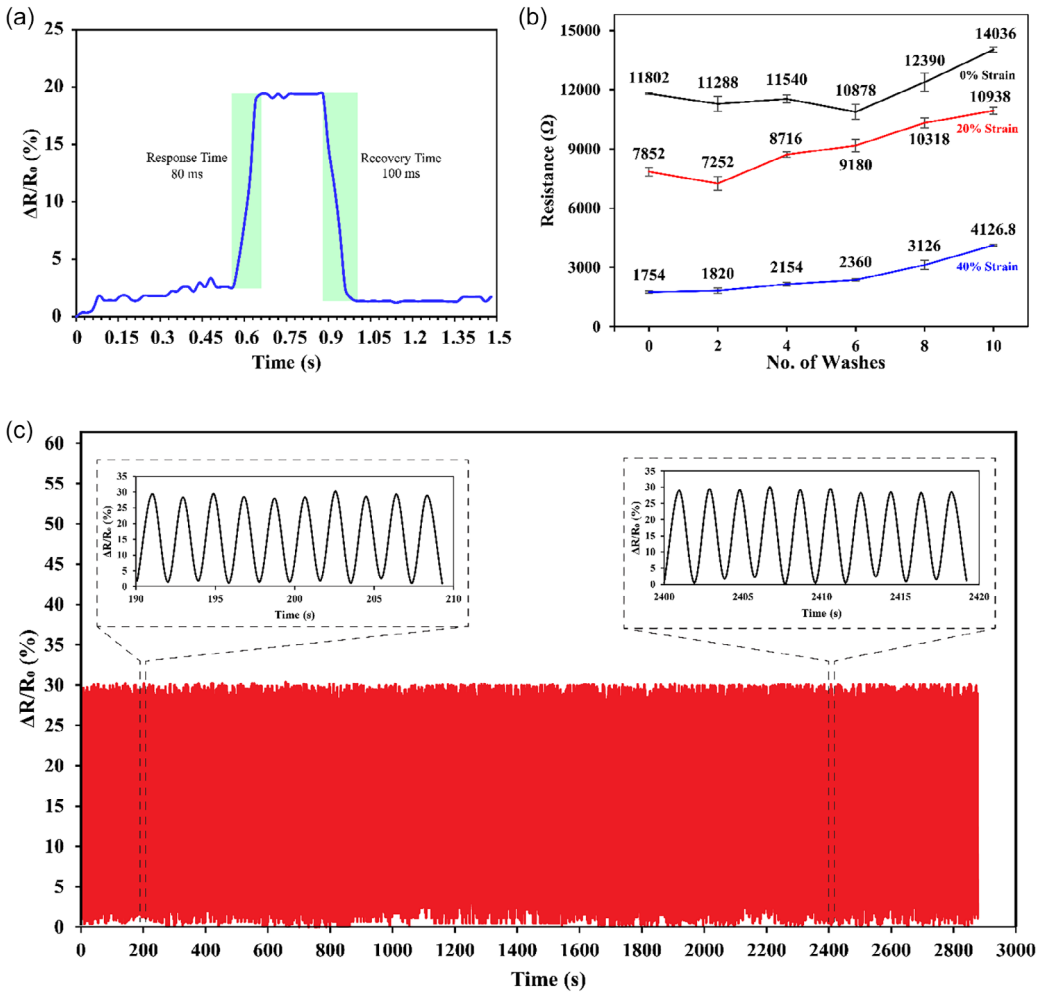


**Figure 4.** Response time, washability, and cyclic stability evaluation of sensor type 4. a) Response-recovery time of the sensor. b) Wash performance up to 10 cycles. c) 1500-cycle stretch-release cyclic test, inset: cyclic test of the sensor during 100–110 cycles (left) and 1250–1260 stretch-release cycles (right). Error bars represent the standard deviation of the measured values ($n = 5$).

other sensor types (Figure S8c–e, Supporting Information) show poor performance, as they exhibit fluctuations in resistance after each pair of wash cycles.

To further evaluate the durability and repeatability of the sensor, a 1500-cycle stretching-releasing cyclic test was performed, as shown in Figure 4c. The sensor underwent 20% strain at 500 mm $min^{-1}$ crosshead speed and was released to come back to its original state for 1500 cycles. The cyclic test shows minimal change in the $\Delta R/R_0$ ratio with no drift over time.[16,24,64] Overall, the developed sensor exhibited outstanding durability and repeatability.

From previous electromechanical characterizations in this study, it can be seen that all sensor types performed similarly in the stability test, sensor types 1 and 4 performed better compared to other sensor types in the variable speed cyclic test, and sensor types 1, 2, and 4 performed better in the washability test. However, sensor type 4 showed the best results in sensitivity (GF = 3.04) and linearity. Thus, sensor type 4 was considered the best among the other 5 sensor types, and the application demonstration proceeded with sensor type 4.

## 3. Comparative Study

This work demonstrates the development of stretchable knitted strain sensors for wireless human motion monitoring applications. Weft knitting technique to fabricate the sensors utilizing commercially available conductive yarns provides high sensitivity, linearity, and good wash performance. Although various fabrication techniques, including knitting, weaving, sewing, braiding, embroidery, have been realized so far,[19,21,22,26,27,58,65–67] our developed sensor shows comparatively better performance. **Table 2** demonstrates various strain sensors and their key performance parameters and has been compared with our developed sensors.

## 4. Application

To show the applicability of the sensors, an elbow support guard and a kneecap were constructed to study their ability in detecting the bending angle of the elbow and knee. To realize this, a 2 × 2

**Table 2.** Performance comparison between various textile-based strain sensors.

| SL | Sensing principle | Functional material | Fabrication method | Gauge factor | Stretching cycle | Linearity ($R^2$) | Wash cycle | Application | Ref. |
|---|---|---|---|---|---|---|---|---|---|
| 1 | Resistive strain sensor | Polyester/stainless steel conductive yarn | Weft knitting | 3.04 | 1500 | 0.9911 | 10 | Walking, jogging, running, cyclic, elbow and knee bending monitoring | [This work] |
| 2 | Resistive strain sensing | Silver-coated nylon yarn | Circular knitting | 3.4 | 600 | – | – | Soft robot gripper for state sensing and tactile feedback | [19] |
| 3 | Resistive strain sensing | Silver-plated nylon yarn | Sewing | 2.08 Ω $mm^{-1}$ (sensitivity) | 100 | 0.997 | – | Walking, running, knee bending monitoring | [21] |
| 4 | Triboelectric effect | Silver-plated Nylon conductive yarn | Braiding | – | – | 0.99 | 25 | Smart elbow guard for sports sensing, military use, high-risk work | [22] |
| 5 | Resistive strain sensing | Silver-plated nylon conductive yarn | Weaving | 2.697 | – | – | – | Hand glove for finger-bending measurement | [26] |
| 6 | Resistive strain sensing | Stainless steel conductive yarn | Embroidery | $1.88 \pm 0.51$ | 100 | 0.898 | – | Soft robotic wearable devices, wearable mechatronic system | [27] |
| 7 | Capacitive strain sensing | Silver-plated nylon yarn | Knitting | 0.68 | 500 | 0.997 | – | Knee brace for walking and cycling monitoring | [58] |
| 8 | Resistive strain sensing | Silver-plated nylon conductive yarn | Sewing | 0.27 | 2000 | 0.98 | – | Hand glove for bending, straining, pressure, and finger support | [65] |
| 9 | Resistive strain sensing | Carbon nanotube | Knitting | $2.93 \times 10^{-3}$ | 30 | 0.9941 | – | Sagittal knee kinematics monitoring | [66] |
| 10 | Resistive strain sensing | Cotton/stainless steel blended yarn | Knitting | 3.7 | – | – | – | – | [67] |

interlock base fabric was fabricated at first using the Shima Seiki SSR 112 flatbed knitting machine. The materials and knitting parameters to fabricate this fabric were also kept the same as the sensor so that the sensor and the base fabric have the same strain and recovery to withstand the load of human limbs. Sensor type 4 was stitched on the base fabric to make the elbow support guard and the kneecap (Figure S9, Supporting Information). **Figure 5**a shows the schematic diagram of the resistance measuring circuit for application demonstration and data acquisition. The process flow of wireless data transmission from the microcontroller to a remote device is shown in Figure 5b. The resistance values in comparison with elbow and knee bending are depicted in Figure 5c,d. The $\Delta R/R_0$ value changes linearly in response to the elbow and knee bending angles. For the elbow support guard, the resistance profile reaches its limit ($\Delta R/R_0 = \approx 91\%$) during a bending angle of 90°. But for the kneecap, the $\Delta R/R_0$ value increases to ≈75%, indicating that it can withstand further knee bending. The sensor's ability to detect bending angles of the elbow and knee has been demonstrated in Videos S1 and S2, Supporting Information. As shown in the videos, three LED lights, blue, green, and red, blink when the elbow and knee bend to 0°, 45°, and 90°, respectively.

Finally, the application of the developed sensor for human motion monitoring was demonstrated. The kneecap was worn, and electrical data was collected during walking, jogging, running, and cycling. All the experiments were done in a real-world environment, that is, in a private gymnasium (Videos S3–S6, Supporting Information). As shown in **Figure 6**a, a single step during walking is distinguishable where the maximum resistance change is ≈25%. The walking speed during the experiment was 5 $kmh^{-1}$. Figure 6b–d shows the change in resistance value during jogging, running, and cycling. In each activity, the sensor can differentiate the human movements by representing the proper electrical response. Maximum resistance changes during jogging, running, and cycling was ≈22%, ≈30%, and ≈10%, respectively. Figure 6e shows the overall acquisition and visualization of the sensor data, from the wearable sensor to the computer app. The sensor is connected to a microcontroller (ESP32), which is powered by a thin battery. The microcontroller and the battery are attached to the kneecap by sewing to prevent falling during various leg movements. The ESP32 collects electrical signals from the sensor and sends the data to a cloud network using the built-in Wi-Fi module. Any designated device, that is, a computer, can access the data and further process it with Python to visualize it in a desktop app. Overall, our developed sensor can detect each segment of the leg movement while running, as depicted in Figure 6e, where the resistance change is the lowest during landing. It then increases slightly and becomes stable momentarily during the loading response, and the highest electrical change is observed when the leg is fully bent during running.

Our sensor, characterized by its lightweight design, affordability, and seamless integration with everyday apparel, possesses significant potential as an objective tool for daily monitoring of posture and gait, as well as the detection of abnormal movements or movement impairments associated with specific neurological disorders and physical rehabilitation. A comprehensive examination of the sensor's performance on the body, with a secondary motion-tracking system, is required to formulate more certain conclusions; nonetheless, the preliminary results seem encouraging.

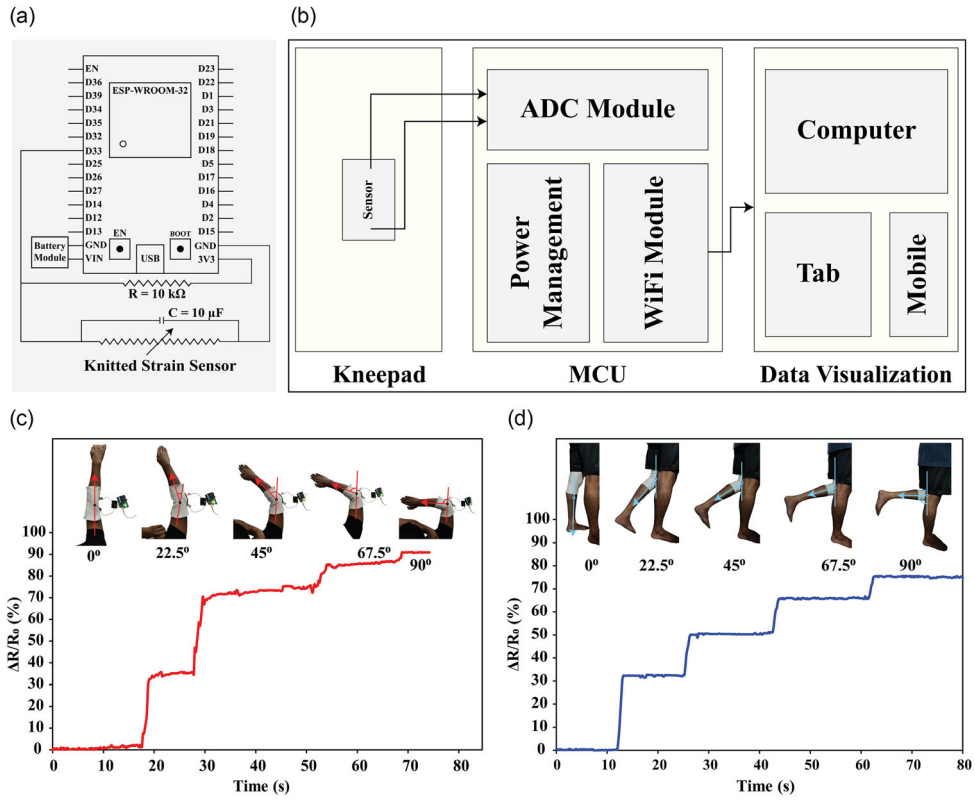


**Figure 5.** Workflow of data collection process for application demonstration and applicability of the developed sensor for elbow and knee bending detection. a) Schematic diagram of resistance value acquisition comprising the voltage divider rule. b) Overview of wireless data transfer from the sensor to the computer via microcontroller. c,d) Resistance profile of the sensor during elbow and knee bending from 0° to 90°.

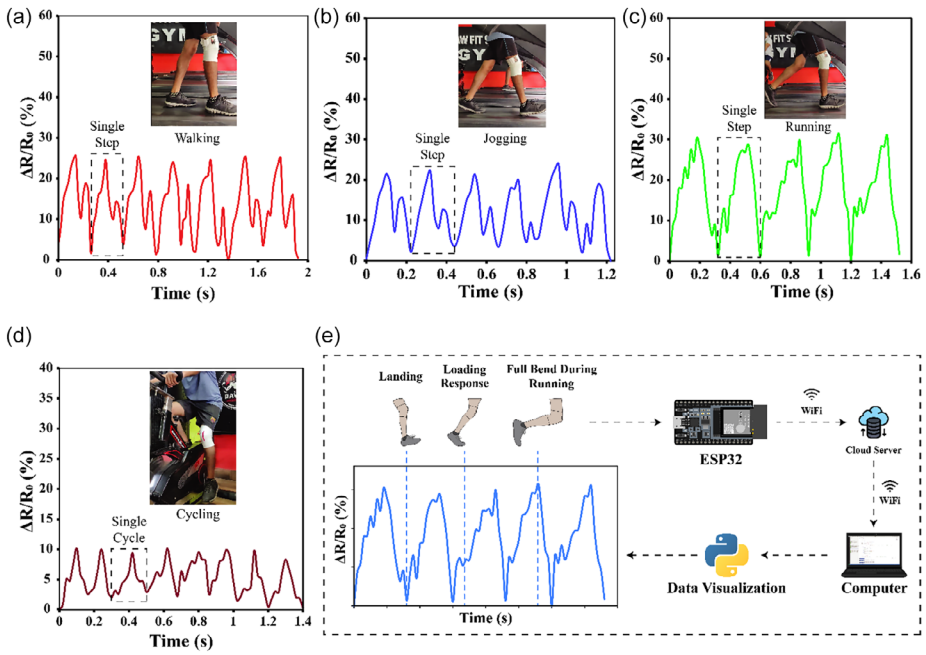


**Figure 6.** Basic real-time sensing application of the resistive strain sensor in human movement monitoring. Visualization of change in $\Delta R/R_0$ in real-time during a) walking, b) jogging, c) running, and d) cycling. e) Breakdown of resistance change in response to knee bending, and live data collection and visualization workflow of the sensor using ESP32 and Python.

## 5. Conclusion

In this work, a fully functional wearable resistive strain sensor has been developed, which is capable of human motion detection. Using a PES/stainless-steel conductive yarn as the functional material, the $2 \times 2$ interlock structure that was fabricated using the Shima Seiki flatbed knitting machine exemplified optimum electromechanical performance. Various electromechanical characterizations proved that sensor 4 exhibited the best results, with a gauge factor of 3.04 and a linearity of 0.9911. The variable-speed cyclic test showed a consistent electrical response, maintaining nearly identical changes in relative resistance during the strain intervals between 0% and 40%. A 1500-cycle stretch-release test further revealed the remarkable durability of the sensor. A lower response time (≈80 ms) and recovery time (≈120 ms), in addition to being practically capable of withstanding up to 10 wash cycles, prove the applicability of the sensors as wearables. The sensor's ability to accurately detect the bending angles further beyond 90° in the form of an elbow guard and kneecap showcases its functional and stable applicability during repeated human locomotion such as walking, jogging, running, cycling, etc. The built-in Wi-Fi module was able to transmit the electrical signals from the sensor through a cloud network to a designated electronic device, enabling the possibility of real-time data transmission and visualization. This lightweight, scalable, seamlessly integrated sensor design can open the doors for more intricate motion detection in potential health monitoring, military, and sports applications.

## 6. Experimental Section

*Materials*: For the fabrication of the strain sensor, PES/stainless steel yarn (400 dtex) sourced from Bekaert, Belgium, was used as the conductive functional material. The yarn has a linear resistance of 13 $\Omega\,cm^{-1}$ and a 60/40 composition of PES and stainless steel fibers. As for the nonconductive base portion, a 300 denier nylon yarn was used, along with a nylon-wrapped spandex yarn (40 denier polyurethane core covered with a 70 denier nylon sheath) purchased from a local market. Both the conductive and nonconductive yarns were used in single plies, as they showcased satisfactory electrical and sensing performance.

*Knitting of the Sensor*: The Shima Seiki SSR112 flat knitting machine was used to fabricate all of the sensors (Figure S10a,b, Supporting Information). Machine parameters for knitting the sensors, that is, stitch length and take-down speed, are given in Figure S11 and S12, Supporting Information.

*Fabrication of Kneepad and Elbow Guard*: To develop the knitted elbow guard and kneepad, a base fabric was knitted using the same parameters that were used to develop the sensors (Figure S10c, Supporting Information). The knitting structure for the base fabric was also $2 \times 2$ interlock. The strain sensor was then sewn onto the base fabric. The knee pad and elbow guard were custom-fitted according to the human subject's elbow and knee measurements.

*Wireless Data Acquisition*: To transmit the sensor data to the computer, the ESP32 microcontroller, which has a built-in Wi-Fi module, has been used. At first, the resistance data acquisition is done by the microcontroller using the voltage divider rule. An additional 10 µF capacitor is connected to the sensor in parallel to receive more stable feedback from the sensor. The ESP32 converts analog strain sensor data to digital signals using the ADC module. The microcontroller is powered by a 3.7 V 600 mAh Li-ion battery, which is managed by a power management module. The built-in Wi-Fi module is used to transfer the data to any computer or mobile device. The Python programming language is used to transfer and visualize the strain sensor data.

*Sensor Characterization*: The developed sensors were characterized by means of various electromechanical tests. A universal testing machine (XFS100) with a load cell of 5 KN was used to collect the mechanical responses of the strain sensor (Figure S13a, Supporting Information). Each sensor was clamped to the tensile tester machine and simultaneously connected to the microcontroller, as depicted in Figure S13b, Supporting Information. A custom-built circuit with a microcontroller (ATmega32u4) was used to measure the resistance of the strain sensors (Figure S14, Supporting Information). Both mechanical and electrical data were collected with a sampling rate of 50 Hz and then synchronized together to use for further electromechanical characterizations. The sensors were characterized in multiple strain ranges (10%, 20%, 30%, and 40%) and various crosshead speeds (50, 100, 150, 200, and 500 mm $min^{-1}$). Relative change in resistance during the experiments was calculated according to the following Equation (3).

$$\frac{\Delta R}{R_0}(\%) = \frac{R_0 - R}{R_0} \times 100\% \tag{3}$$

where $\Delta R$ denotes the change in resistance, $R_0$ denotes the initial resistance, and $R$ denotes the current resistance while stretching. All samples underwent a 24 h relaxation period before the tests, which took place at a room temperature of 24 °C. Furthermore, all tests were conducted at a 24 °C temperature and a relative humidity of 65%.

## Supporting Information

Supporting Information is available from the Wiley Online Library or from the author.

## Acknowledgements

The research has been done at the Smart and Functional Textiles Lab, Department of Fabric Engineering, Bangladesh University of Textiles (BUTEX). All authors acknowledge the authorities of Bangladesh University of Textiles for giving the opportunity to complete this research. All participants provided written informed consent before participation in the experiments.

## Conflict of Interest

The authors declare no conflict of interest.

## Data Availability Statement

The data that support the findings of this study are available from the corresponding author upon reasonable request.

## Keywords

flat knitting, human motion monitoring, smart textiles, strain sensors, wireless monitoring

Received: August 10, 2025
Revised: November 5, 2025
Published online:

[1] J. Shi, S. Liu, L. Zhang, B. Yang, L. Shu, Y. Yang, M. Ren, Y. Wang, J. Chen, W. Chen, Y. Chai, X. Tao, *Adv. Mater.* **2020**, *32*, 1901958.
[2] L. Liu, X. Liang, X. Wan, X. Kuang, Z. Zhang, G. Jiang, Z. Dong, C. Chen, H. Cong, H. He, *Adv. Mater. Technol.* **2023**, *8*, 2300820.
[3] Y. Chen, Z. Deng, R. Ouyang, R. Zheng, Z. Jiang, H. Bai, H. Xu, *Nano Energy* **2021**, *84*, 105866.

 

[4] J. Stanley, K. Griggs, O. Handford, J. A. Hunt, P. Kunovski, Y. We, *Proc. of the 2022 ACM Inter. Symp. on Wearable Computers*, Association for Computing Machinery, New York, NY **2022**, pp. 131–135.
[5] Y. Li, R. Takahashi, W. Yukita, K. Matsutani, C. Caremel, Y. Iwamoto, S. Lee, T. Yokota, T. Someya, Y. Kawahara, *Proc. of the Nineteenth Inter. Conf. on Tangible, Embedded, and Embodied Interaction*, Association for Computing Machinery, New York, NY **2025**.
[6] B. Zhao, Z. Dong, H. Cong, *Sens. Actuators A Phys.* **2022**, *340*, 113558.
[7] Md. M. Hosen, S. Ahmed, *J. Eng. Fiber Fabr.* **2025**, *20*, 15589250251331051.
[8] S. Sun, Y. Liu, X. Chang, Y. Jiang, D. Wang, C. Tang, S. He, M. Wang, L. Guoa, Y. Gao, *J. Mater. Chem. C* **2020**, *8*, 2074.
[9] H. R. Nejad, M. P. Punjiya, S. Sonkusale, in *2017 19th Inter. Conf. on Solid-State Sensors, Actuators and Microsystems (TRANSDUCERS)* **2017**, pp. 1183–1186.
[10] J. Tolvanen, J. Hannu, H. Jantunen, *Sci. Rep.* **2018**, *8*, 13241.
[11] T. Alam, F. Saidane, A. al Faisal, A. Khan, G. Hossain, *Sens. Actuators A Phys.* **2022**, *341*, 113587.
[12] G. Chen, X. Xiao, X. Zhao, T. Tat, M. Bick, J. Chen, *Chem. Rev.* **2022**, *122*, 3259.
[13] M. Dulal, H. R. M. Modha, J. Liu, M. R. Islam, C. Carr, T. Hasan, R. M. S. Thorn, S. Afroj, N. Karim, *Energy Environ. Mater.* **2025**, *8*, e12854.
[14] W. Fan, Q. He, K. Meng, X. Tan, Z. Zhou, G. Zhang, J. Yang, Z. L. Wang, *Sci. Adv.* **2020**, *6*, eaay2840.
[15] M. Zahid, A. Zych, S. Dussoni, G. Spallanzani, R. Donno, M. Maggiali, A. Athanassiou, *Compos. B Eng.* **2021**, *220*, 108969.
[16] M. A. Rumon, G. Cay, V. Ravichandran, A. Altekreeti, A. Gitelson-Kahn, N. Constant, D. Solanki, K. Mankodiya, *Biosensors* **2023**, *13*, 34.
[17] T. Lim, H. J. Kim, S. Won, C. H. Kim, J. Yoo, J. H. Lee, K. S. Son, I. Nam, K. Kim, S. Y. Yeo, B. J. Yeang, J. H. Kim, H. Zhang, S. Lee, *ACS Appl. Nano Mater.* **2023**, *6*, 8482.
[18] S. Afroj, N. Karim, Z. Wang, S. Tan, P. He, M. Holwill, D. Ghazaryan, A. Fernando, K. S. Novoselov, *ACS Nano* **2019**, *13*, 3847.
[19] M. Yang, F. Sun, X. Hu, F. Sun, *ACS Appl. Mater. Interfaces* **2023**, *15*, 44294.
[20] A. Javaid, M. H. Zulfiqar, M. S. Saleem, M. A. Khan, M. Zubair, Y. Massoud, M. Q. Mehmood, *Adv. Eng. Mater.* **2024**, *26*, 2301138.
[21] A. K. Aliyana, D. Yang, O. Tangsirinaruenart, G. K. Stylios, *Results Eng.* **2024**, *23*, 102794.
[22] K. Wang, Y. Shen, T. Wang, Z. Li, B. Zheng, Z. Dong, F. Ning, G. Jiang, G. Zhao, C. Chen, P. Ma, *Adv. Fiber Mater.* **2024**, *6*, 786.
[23] L. Li, J. Sun, H. Cong, *J. Indust. Text.* **2023**, *53*, 15280837231200895.
[24] U. Gupta, J. L. Lau, P. Z. Chia, Y. Y. Tan, A. Ahmed, N. C. Tan, G. S. Soh, H. Y. Low, *Adv. Healthc. Mater.* **2023**, *12*, 2202987.
[25] Y. Li, X. Miao, R. K. Raji, *Smart Mater. Struct.* **2019**, *28*, 115042.
[26] L. Fang, Z. Dong, M. Zhang, Z. Sun, X. Wu, Y. Wu, L. Yu, R. Sun, H. Zhao, L. Qian, C. Ying, *J. Indust. Textiles* **2023**, *53*, 15280837231222622.
[27] J. G. Colli Alfaro, A. L. Trejos, *Sensors* **2023**, *23*, 1503.
[28] T. Caliskan, A. Arslan, B. Kostekci, M. Kumru, M. A. Kalafat, I. Gocek, *Mater. Today Proc.* **2023**, *93*, 79.
[29] M. R. Islam, S. Afroj, K. S. Novoselov, N. Karim, *Adv Funct. Mater.* **2024**, *34*, 2410666.
[30] J. Hughes, A. Spielberg, M. Chounlakone, G. Chang, W. Matusik, D. Rus, *Adv. Intell. Syst.* **2020**, *2*, 2000002.
[31] S. Lu, S. Wang, G. Wang, J. Ma, X. Wang, H. Tang, X. Yang, *Sens. Actuators A Phys.* **2019**, *295*, 200.
[32] A. Yadav, N. Yadav, Y. Wu, S. R. Krishna, Z. Hongyu, *Mater. Adv.* **2023**, *4*, 1444.
[33] L. Shi, J. Feng, Y. Zhu, F. Huang, K. Aw, *Sens. Actuators A Phys.* **2024**, *377*, 115730.
[34] M. Amjadi, K.-U. Kyung, I. Park, M. Sitti, *Adv. Funct. Mater.* **2016**, *26*, 1678.
[35] X. He, G. Shen, J. Liang, Z. Liu, Y. Xin, T. Liang, J. He, C. Zhang, Y. Chen, X. He, *ACS Appl. Electron. Mater.* **2021**, *3*, 3287.
[36] P. Kateb, A. Fornaciari, C. Ahmadizadeh, A. Shokurov, F. Cicoira, C. Menon, *Adv. Intel. Syst.* **2024**, *6*, 2400292.
[37] M. Tavassolian, T. J. Cuthbert, C. Napier, J. Peng, C. Menon, *Adv. Intel. Syst.* **2020**, *2*, 1900165.
[38] V. Galli, S. K. Sailapu, T. J. Cuthbert, C. Ahmadizadeh, B. C. Hannigan, C. Menon, *Adv. Sci.* **2023**, *10*, 2206665.
[39] D.-H. Kang, J.-H. Lee, J.-W. Lee, H. Cho, S. Park, K. Lee, S. Kang, *J. Med. Syst.* **2021**, *45*, 41.
[40] F. Xu, S. Dong, G. Liu, C. Pan, Z. H. Guo, W. Guo, L. Li, Y. Liu, C. Zhang, X. Pu, Z. L. Wang, *Nano Energy* **2021**, *88*, 106247.
[41] Y. Xiong, L. Luo, J. Yang, J. Han, Y. Liu, H. Jiao, S. Wu, L. Cheng, Z. Feng, J. Sun, Z. L. Wang, Q. Sun, *Nano Energy* **2023**, *107*, 108137.
[42] T. Dong, Y. Gu, T. Liu, M. Pecht, *Sens. Actuators A Phys.* **2021**, *326*, 112720.
[43] R. Nur, N. Matsuhisa, Z. Jiang, M. O. G. Nayeem, T. Yokota, T. Someya, *Nano Lett.* **2018**, *18*, 5610.
[44] Z. Luo, N. Kong, K. A. S. Usman, J. Tao, P. A. Lynch, J. M. Razal, J. Zhang, *Polymers* **20241824**, *16*.
[45] B. Bozali, S. Ghodrat, L. Plaude, J. J. F. Dam, K. M. B. Jansen, *Sensors* **2022**, *22*, 7688.
[46] C. Fan, Y. Liu, Y. Zhang, *Adv. Fiber Mater.* **2024**, *6*, 1152.
[47] A. K. Stavrakis, M. Simić, M. Damnjanović, G. M. Stojanović, *Heliyon* **2024**, *10*, e26069.
[48] Y. Zhou, Y. Sun, Y. Li, C. Shen, Z. Lou, X. Min, R. Stewart, *Adv. Intel. Syst.* **2024**, *6*, 2400124.
[49] M. M. Hossain, M. M. Lubna, P. D. Bradford, *ACS Appl. Mater. Interfaces* **2023**, *15*, 3365.
[50] Z. Tang, S. Jia, F. Wang, C. Bian, Y. Chen, Y. Wang, B. Li, *ACS Appl. Mater. Interfaces* **2018**, *10*, 6624.
[51] Y. Zhou, C. Myant, R. Stewart, *J. Appl. Polym. Sci.* **2022**, *139*, e52755.
[52] S. Seyedin, S. Moradi, C. Singh, J. M. Razal, *Appl. Mater. Today* **2018**, *11*, 255.
[53] Y. Guo, X. Wei, S. Gao, W. Yue, Y. Li, G. Shen, *Adv. Funct. Mater.* **2021**, 31.
[54] A. Georgopoulou, F. Clemens, *ACS Appl. Electron. Mater.* **2020**, *2*, 1826.
[55] C. Yan, J. Wang, W. Kang, M. Cui, X. Wang, C. Y. Foo, K. J. Chee, P. S. Lee, *Adv. Mater.* **2014**, *26*, 2022.
[56] S. Lee, *J. Eng. Fiber Fabr.* **2022**, *17*, 15589250221104474.
[57] Q. Chen, L. Shu, B. Fu, R. Zheng, J. Fan, *Polymers* **2021**, *13*, 1015.
[58] S. Seyedin, J. M. Razal, P. C. Innis, A. Jeiranikhameneh, S. Beirne, G. G. Wallace, *ACS Appl. Mater. Interfaces* **2015**, *7*, 21150.
[59] A. F. Yilmaz, I. A. K. Ahmed, C. Gumus, K. Ozlem, M. S. Cetin, A. T. Atalay, G. Ince, O. Atalay, *Adv. Sens. Res.* **2024**, *3*, 10.
[60] O. Atalay, *Materials* **2018**, *11*, 768.
[61] R. Holm, *Electric Contacts*, 4th ed., Springer Berlin Heidelberg, Berlin, Heidelberg **1967**.
[62] Y. Luo, K. Wu, T. S. Palacios, W. Matusik, *Conf. on Human Factors in Computing Systems - Proceedings*, Association for Computing Machinery **2021**, pp. 1–12.
[63] M. M. Hosen, A. Ferdous, S. Ahmed, *J. Indus. Text.* **2024**, 54.
[64] X. Zhou, C. Hu, X. Lin, X. Han, X. Zhao, J. Hong, *Sens. Actuators A Phys.* **2021**, *321*, 112591.
[65] A. F. Yilmaz, K. Ozlem, F. Khalilbayli, M. F. Celebi, F. Kalaoglu, A. T. Atalay, G. Ince, O. Atalay, *Adv. Sens. Res.* **2024**, 3.
[66] C. D. Fay, N. Mannering, A. Jeiranikhameneh, F. Mokhtari, J. Foroughi, R. H. Baughman, P. F. M. Choong, G. G. Wallace, *Adv. Sens. Res.* **2023**, *2*, 2200021.
[67] J. Xie, H. Long, M. Miao, *Smart Mater. Struct.* **2016**, *25*, 105008.